



# Molecular Insights on the Role of $(\text{CTA}^+)(\text{SiO}^-)$ Ion Pair into the Catalytic Activity of $[\text{CTA}^+]\text{-Si-MCM-41}$

Clara Iris Aymar Alegre<sup>1,2</sup> · Marıa Fernanda Zalazar<sup>1,2</sup> · Barbara Bulhoes Cazula<sup>3</sup> · Helton Jose Alves<sup>3</sup> · Nelida Marıa Peruchena<sup>1,2</sup>

 Springer Science+Business Media, LLC, part of Springer Nature 2019

## Abstract

In this work, a theoretical study in conjunction with a spectroscopic analysis by FTIR were carried out in order to obtain molecular insights on the role of  $(\text{CTA}^+)(\text{SiO}^-)$  ion pair into the catalytic activity of  $[\text{CTA}^+]\text{-Si-MCM-41}$ , the non-calcined form of Si-MCM-41. The reaction of transesterification of ethyl acetate with methanol was used as a model of transesterification of vegetal oils using the mesoporous heterogeneous catalyst. The theoretical study was performed in the framework of density functional theory (DFT) in order to provide new insights that could be helpful in the understanding of these chemical reactions on solid surfaces. It is found that the most favorable reaction mechanism is the dual site mechanism and that the presence of the  $(\text{CTA}^+)(\text{SiO}^-)$  ionic pair is fundamental for the catalytic activity. The basic center of  $[\text{CTA}^+]\text{-Si-MCM-41}$  catalyst polarizes the adsorbed methanol and the acid center polarizes the carbonyl of adsorbed ethyl acetate. Thus, this bifunctional catalytic site makes possible the concerted adsorption of both reactants at the pore mouth and generates a concerted transition state that gives rise to the beginning of the transesterification reaction and the formation of the unstable tetrahedral intermediate which will give rise to the products.

**Keywords** Bifunctional catalytic site · Transesterification reaction · Concerted adsorption · Heterogeneous basic catalysis · DFT

## 1 Introduction

The selective transformation of raw materials derived from renewable biomass plays a key role in the production of sustainable biofuels and fine chemicals substances [1].

**Electronic supplementary material** The online version of this article (<https://doi.org/10.1007/s11244-019-01181-2>) contains supplementary material, which is available to authorized users.

✉ Marıa Fernanda Zalazar  
mfzalazar@conicet.gov.ar

<sup>1</sup> Laboratorio de Estructura Molecular y Propiedades (LeMYP), Facultad de Ciencias Exactas, Naturales y Agrimensura, Universidad Nacional del Nordeste (UNNE), Avenida Libertad 5460, 3400 Corrientes, Argentina

<sup>2</sup> Instituto de Quımica Basica y Aplicada del Nordeste Argentino, IQUIBA-NEA, CONICET-UNNE, Avenida Libertad 5460, 3400 Corrientes, Argentina

<sup>3</sup> Laboratorio de Catalise e Producao de Biocombustıveis (LabCatProBio), Universidade Federal do Parana (UFPR – Setor Palotina), Palotina, Brazil

Usually, the processes employed in biomass conversion are catalytic and may require high temperatures and/or pressure in order to achieve good yields. In this context, the search for catalysts with high activity and selectivity generates considerable interest and is a vast field for research. In this research field, we can find for example zeolites and molecular sieves of the M41S family. The last ones are synthesized under hydrothermal conditions from a silica source, water, a mineralizing agent and an ionic surfactant as template [2], such as materials with the MCM-41 structure.

During the synthesis of mesoporous Si-MCM-41, the micelles of the organic surfactant are used as a structure-directing agent (SDA), around which the silicate species present in the reaction mixture are organized to form an ordered mesostructure, which balances the charge on the micellar surfaces. Then, this material is calcined in order to remove the SDA that is located inside the pores, generating finally a solid with a high specific area that is composed only by amorphous silica with a mesoporous hexagonal arrangement chemically inert, which limits its application as a catalyst.

Thus, it is necessary sometimes to functionalize the solid surface with amines, metals such as titanium and aluminum or metal oxides [3].

Previous experimental works reported the use of MCM-41 without calcination, where the organic SDA has been kept occluded, as a basic solid catalyst potentially usable for several reactions [4–8]. Kubota et al. reported that the high activity of Si–MCM-41 with a quaternary ammonium ion occluded emerges only when both parts form a composite [4]. Martins and co-workers studied the Knoevenagel condensation reaction using Si–MCM-41 molecular sieves as basic catalyst, where the pores were occluded by the SDA, and suggested from  $^{29}\text{Si}$  NMR spectroscopy and O1s XPS measurements, that the active site is the  $\equiv\text{SiO}^-\text{CTA}^+$  ionic pair, which is the basic site itself, also they suggested that the reaction should occur in the pore mouth [5]. Other work showed that different mesoporous materials synthesized with surfactants of different lengths in the carbon chain ensure greater catalytic activity when the occluded cation is more voluminous, this was attributed to the more weaker interaction with  $\text{SiO}^-$  sites, thus increasing the  $\text{SiO}^-$  basicity [9].

Also good yields were found for the reaction of transesterification of vegetable oils for the biodiesel production using heterogeneous Si–MCM-41 molecular sieves in the non-calcined form, denoted as  $[\text{CTA}^+]\text{--Si--MCM-41}$  catalysts, where the cetyltrimethylammonium cation ( $\text{CTA}^+$ ) from the structure-directing agent was not removed from the formed catalyst [6]. Further results also showed that the catalyst without the occluded surfactant and the surfactant itself does not possess catalytic activity when were used separately, suggesting that the interaction between the  $\text{CTA}^+$  and the mesoporous silica is responsible for the catalytic activity in the transesterification reaction [10]. Also, some studies reported that when the  $[\text{CTA}^+]\text{--MCM-41}$  catalyst was recovered after a reaction cycle and reused, then the catalytic activity was reduced progressively as the number of reaction cycles increased, which showed that the surfactant was being leached to the reactional media and perhaps during the washing after the reaction, and the activity lost was attributed to the template extraction [3, 6, 10]. Hence, such activity was associated with the formation of  $(\text{CTA}^+)(\equiv\text{SiO}^-)$  ion pair at the surface of the solid catalyst and was postulated that the basic active sites resided at the pore mouth. But, despite the good yields reported for the reaction, there is no further information available on the basic properties of the formed catalyst.

However, there is still a need for works supporting this experimental observation, which is currently a topic of debate since, by modifying the synthesis conditions of these materials, materials with different textural properties and catalytic activity can be obtained. This can be related to a

compromise between the formation of the  $(\text{CTA}^+)(\equiv\text{SiO}^-)$  ion pair which is suggested from the experimental viewpoint that is crucial for the catalytic activity.

Beyond that the transesterification mechanisms of vegetal oils by homogeneous catalysts are well understood, the reactions mechanisms of oils catalyzed by heterogeneous catalyst have not been dealt with in depth because of the complexity of the study of the surface-reactants system. In heterogeneous catalysis, the adsorption is the first step that initiates the reaction, and in general, the reactant molecules are adsorbed in very different ways due to the huge complexity of the solid surfaces [11, 12]. Although, MCM-41 material is very commonly used as a support for catalysts, nevertheless, theoretical studies are limited. This is explained by the lack of appropriate models that accurately describe the real material and because of the computational cost of simulates mesoporous materials [13]. Also, about transesterification reactions using  $[\text{CTA}^+]\text{--Si--MCM-41}$  catalyst, remains unclear the involved mechanism and the role of  $(\text{CTA}^+)(\equiv\text{SiO}^-)$  ion pair, geometries of adsorbed species and reaction intermediates, interactions between adsorbate-catalyst, among others.

Additionally, computational approaches can be applied to gain novel and valuable molecular insights into adsorption mechanisms and catalysis [14]. A recent review highlighted the combination of theoretical and experimental techniques applied to describe the reaction mechanisms, for example, FTIR spectra have been interpreted with the help of the DFT calculation in order to describe adequate chemical models of interacting systems [15].

From our perspective, the catalytic problem comprises a highly interdisciplinary topic that includes concepts and contributions from all areas of chemistry in order to increase the scientific knowledge. As a result, an elaborate understanding of the mechanism in catalyzed heterogeneous reactions is prerequisite in order to shed light on the experimental results, the theories, and also for the optimization of the processes and the development of new catalysts that imitating nature, being so efficient and specific as biological catalysts.

The aim of this study is to examine at the molecular level that occurs on the surface of the catalyst, what is the effect of the occluded surfactant and the role of  $(\text{CTA}^+)(\equiv\text{SiO}^-)$  ion pair on the catalytic activity of  $[\text{CTA}^+]\text{--Si--MCM-41}$ . The reaction of transesterification of ethyl acetate (which is the simplest known ester) with methanol was used as a model of transesterification of vegetal oils. The reaction mechanism on the surface of the catalyst is also explored at molecular level in order to provide new insights to increase our understanding of these chemical reactions. Spectroscopic analysis of catalyst by FT-IR were performed for purposes of comparison with theoretical data.

## 2 Method and Calculation Details

### 2.1 The MCM-41 Model

The mesoporous silica models were built based on pure Si-MCM-41 silanol-terminated surface structure reported by Ugliengo et al. [16]. Because the large size of the mesoporous silica with pores of about 30–40 Å across the structure and walls about 10 Å thick (Fig. 1a) [16], the catalyst was modeled with two different cluster model consisting of 6 and 10 SiO<sub>4</sub> tetrahedra denoted as 6T or 10T (where T represents tetrahedral atoms of Si) in order to treating them as two separate adsorption sites (Fig. 1b, c). The cluster model was cut out from the surface wall and the dangling bonds were saturated with H atoms at a bond length of 1.47 Å from the silicon atoms and orientated towards the corresponding Si–O bonds of the silica framework.

### 2.2 Model of Structure-Directing Agent

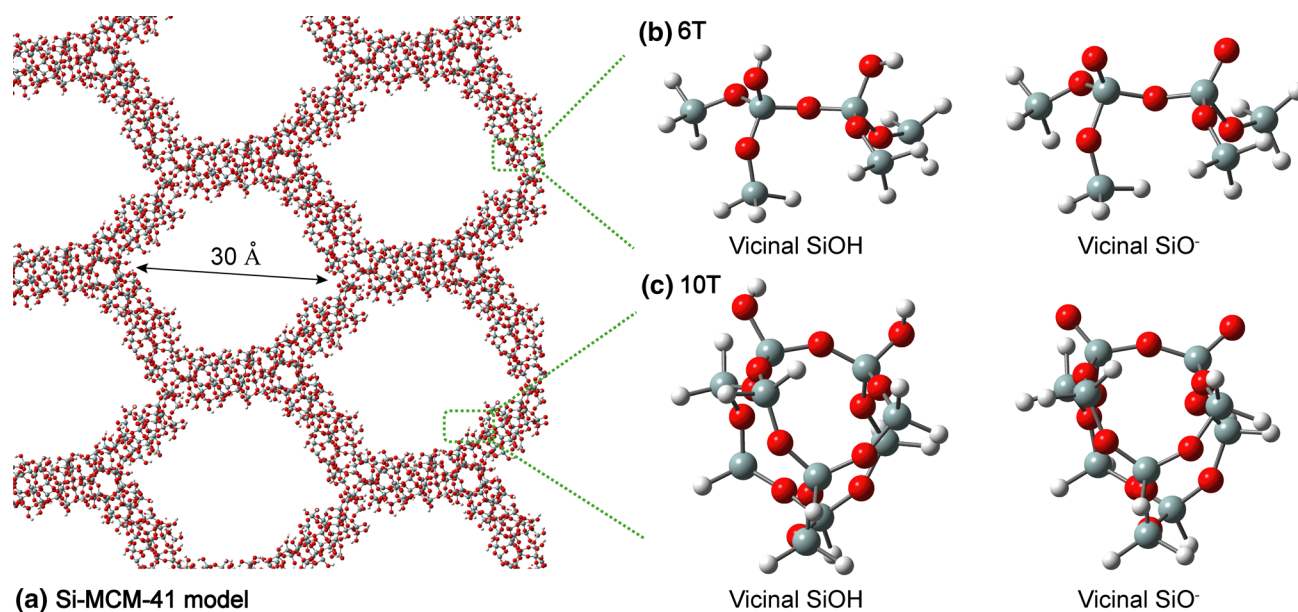
From experimental viewpoint, the Si-MCM-41 molecular sieve is synthesized by the cetyltrimethylammonium bromide (CTA-Br) as the structure-directing agent. The cetyltrimethylammonium cation C<sub>16</sub>TA<sup>+</sup> was model with a C<sub>n</sub>TA<sup>+</sup> cation (n = 4, 6). See Figure S1 of supporting information section.

### 2.3 Model of [CTA<sup>+</sup>]-Si-MCM-41 Catalyst

According to experimental results by Martins and co-workers, the siloxy groups, SiO<sup>−</sup>M<sup>+</sup>, are not hydrogen-bonded, but they are present major as ≡SiO<sup>−</sup>CTA<sup>+</sup> ionic pairs, generating SiO<sup>−</sup> basic sites [5]. The model surface was built using a CTA<sup>+</sup> cation coupled on the silicate cluster (6T and 10T), in which the electrical neutrality of the ion pair is preserved. This proposal is based on experimental results that showed that for each removed CTA<sup>+</sup>, a silanol group is generated in the solid [5]. Then, when the silicate model contains two free siloxy anions, two pairs of CTA<sup>+</sup> cations are coupled. This model also is considered as the surface of the pore mouth where it has been postulated that the reaction occurs (because experimental results show that [CTA]-Si-MCM-41 pores are completely filled with the surfactant agent, thus it was postulated that the reaction occurs on the pore mouth). The distance of the terminal hydrogens (H<sub>t</sub>) was set at 6 and 5 Å (for 10T and 6T model respectively) to avoid separation of the two surfactant chains by repulsion and thus simulate the surface.

### 2.4 Computational Details

Hybrid density functional theory (DFT) calculations at the Becke3 Lee–Yang–Parr (B3LYP) level [17, 18] with the 6-31G(d,p) basis set were carried out using the Gaussian09 software [19]. This functional was previously used to model amorphous silica surfaces [16, 20]. All stationary points were characterized by calculating the Hessian matrix and



**Fig. 1** a Structure of Si-MCM-41 model by Ugliengo [16]. b, c Models of two possible silica surface sites, where vicinal SiOH refers to a hydroxylated form with two adjacent silanol groups (Si–OH) and vicinal SiO<sup>−</sup> refers to a model with two siloxys (≡SiO<sup>−</sup>) groups

analyzing the vibrational normal modes. Relative infrared intensities ( $I_{\text{IR}}$ ) in % were obtained by normalizing the computed value to the intensity of the strongest band. Intrinsic reaction coordinate (IRC) calculations were performed to unambiguously confirm the connection between reactants and products. The reaction path was followed employing the IRC algorithm [21, 22], as implemented in Gaussian 09. A step size of  $0.01 \text{ amu}^{-1/2} \text{ bohr}$  was used according to previous work [23]. The van der Waals interactions between reactant species were taken into account by including Grimme's—D3 dispersion corrections, DFT-D3 [24].

Interaction energy ( $\Delta E_{\text{int}}$ ) of ion-pair [CTA<sup>+</sup>]-MCM-41 was calculated via Eq. (1):

$$E_{\text{int}} = E_{\text{ion\_pair}} - (E_{\text{SiO}^-} + n \times E_{\text{CTA}^+}) \quad (1)$$

where  $E_{\text{ion\_pair}}$  is the total energy of the optimized ion pair (CTA<sup>+</sup>)(≡SiO<sup>-</sup>),  $E_{\text{SiO}^-}$  is the total energy of the mesoporous silica cluster model (6T or 10T, respectively),  $n$  represents the number of surfactant molecules involved in the formation of the ion pair and  $E_{\text{CTA}^+}$  is the total energy of the optimized cation C<sub>n</sub>TA<sup>+</sup> [(C<sub>4</sub>TA<sup>+</sup>) or (C<sub>6</sub>TA<sup>+</sup>) according to the considered model].

Adsorption energies ( $\Delta E_{\text{ads}}$ ) were computed via Eq. (2) as the differences between the total energy of the optimized adsorbed complex,  $E_{\text{adsorbed complex}}$ , and the sum of the total energies of the isolated reactant molecules,  $E_{\text{reactant}}$ , and the catalyst model,  $E_{\text{catalyst}}$ :

$$E_{\text{ads}} = E_{\text{adsorbed complex}} - (E_{\text{reactant}} + E_{\text{catalyst}}) \quad (2)$$

Deprotonation energy of methanol ( $\Delta E_{\text{DPM}}$ ) was calculated via Eq. (3).

$$E_{\text{DPM}} = E_{\text{MeO}^-} - E_{\text{ads\_MeOH}} \quad (3)$$

where  $E_{\text{MeO}^-}$  is the energy of methoxide species. Activation energies ( $E_{\text{a}}$ ) were calculated as the energies differences between the transition state and the adsorbed complex.

Total electron densities were obtained at B3LYP level using a 6-31++G(d,p) basis set, and the Gaussian program. The maps of molecular electrostatic potential (MEP) of the catalyst model were calculated and drawn with AIMAll software [25] using a 0.001 au electron density isosurface.

## 2.5 Experimental

Samples of [CTA<sup>+</sup>]-Si-MCM-41 (non-calcined) and Si-MCM-41 (calcined) were synthesized according to the method described by Grün [2], using a cation of Cetyl Trimethyl Ammonium (CTA<sup>+</sup>) as the mesoporous structure-directing agent. As the synthesis occurs in aqueous medium, the following reagents were used: cetyltrimethylammonium bromide (CTA-Br), ammonium hydroxide (NH<sub>4</sub>OH) as the

mineralizing agent, tetraethylorthosilicate (TEOS) as the silica source, deionized water and absolute ethanol as solvent and co-solvent. The synthesis procedure was described in our previous works [6, 10].

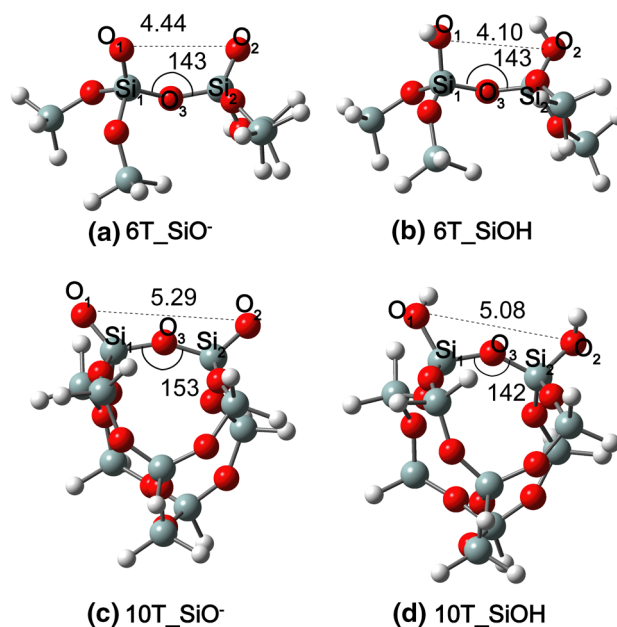
The experimental analyzes of Fourier Transform Infrared Spectroscopy (FT-IR) were performed on pure samples of Si-MCM-41 (calcined) and [CTA<sup>+</sup>]-Si-MCM-41 (non-calcined), and were carried out in equipment model PerkinElmer Spectrum 65 equipped with an ATR accessory. The spectra were obtained in the range of 600 to 4000 cm<sup>-1</sup>, with resolution of 0.5 cm<sup>-1</sup>.

## 3 Results and Discussion

### 3.1 MCM-41 Catalyst Model

Figure 2 shows the optimized structures for 6T and 10T models of MCM-41 catalyst.

The 6T\_SiO<sup>-</sup> model contains two terminal siloxy groups (angle Si<sub>1</sub>-O<sub>3</sub>-Si<sub>2</sub> = 143° and distance O<sub>1</sub>...O<sub>2</sub> = 4.44 Å, Fig. 2a). The walls of the MCM-41 structure are of amorphous nature, and they are formed from the tempered of the used surfactant, therefore, to give rise to such variation two different positions of the structure presented by Ugliengo were used [16]. The 10T\_SiO<sup>-</sup> model was cut off considering a closed silica ring in order to consider the tension of the ring. In this model the Si<sub>1</sub>-O<sub>3</sub>-Si<sub>2</sub> angle is 153°, giving rise to a O<sub>1</sub>...O<sub>2</sub> distance of 5.29 Å, Fig. 2c, this longer distance will allow an



**Fig. 2** Main geometrical parameters of optimized 6T and 10T models for two different sites of MCM-41 catalyst, **a, c** non-hydroxylated and **b, d** hydroxylated silica model

ion-pair model with more open CTA<sup>+</sup> structures. The model with two silanol-terminated surfaces simulates the hydroxylated MCM-41 material (calcined catalyst), Fig. 2b, d.

### 3.2 Model of [CTA<sup>+</sup>]-Si-MCM-41 Catalyst (Non-calcined Catalyst) or Ion-Pair Model

From the CTA-Br surfactant, the silica source (tetraethoxysilane or TEOS) is accommodated over the head of the CTA<sup>+</sup> cation, giving rise to the [CTA<sup>+</sup>]-Si-MCM-41 catalyst or non-calcined catalyst. The synthesis is a sol-gel reaction that occurs by hydrolysis followed condensation, the residual organic part of TEOS forms ethanol that is then removed in the wash of the gel, giving rise to the synthesized non-calcined catalyst, according to the following reactions:

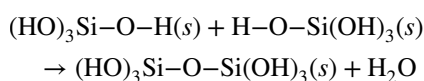
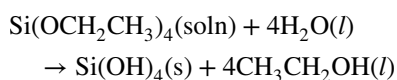
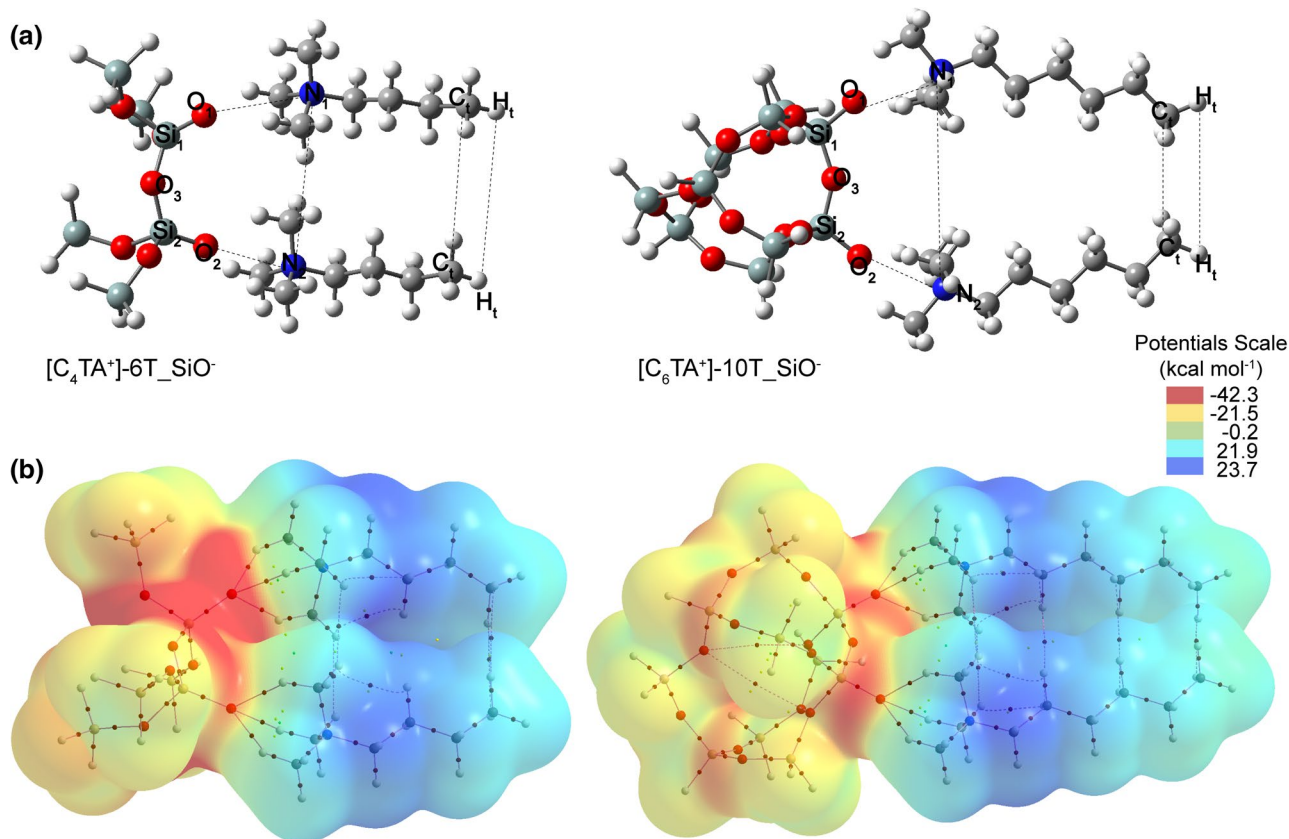


Figure 3 shows the most stable structures for different ion-pair models of [CTA<sup>+</sup>]-Si-MCM-41 and Table 1 shows their main geometrical parameters.

It can be observed that the head of the two surfactant cations are oriented towards the negatively charged siloxy groups giving rise to the ion-pair model. One difference lies in the structure and size of the silica aggregate (6T vs. 10T), in both models the SiO<sup>-</sup>/SiO<sup>-</sup> terminals are each linked by an anion of surfactant so that the total charge of the ion-pair is zero. As expected in the ion-pair, due to the greater separation of the siloxy anions the two heads of surfactant are more separated giving rise to different models of catalyst aggregate. It can be observed that geometrical parameters involved in the interaction (O<sub>1</sub>...N<sub>1</sub> and O<sub>2</sub>...N<sub>2</sub>) does not significantly differ for both models, which involve different silica aggregates (6T vs. 10T) and long carbon chain in the surfactant (4 vs. 6 carbon atoms). However, N<sub>1</sub>...N<sub>2</sub> distance differs as can be expected. The interaction energies are -257.7 versus -232.3 kcal mol<sup>-1</sup> (6T vs. 10T).

MEPs based on electron density provide valuable information about the shape, volume, and electronic properties of



**Fig. 3** **a** Most stable structures for two different ion-pair models of [CTA<sup>+</sup>]-Si-MCM-41. **b** Molecular electrostatic potential on the 0.001 au. electron density isosurface for [C<sub>4</sub>TA<sup>+</sup>]-6T-SiO<sup>-</sup> and [C<sub>6</sub>TA<sup>+</sup>]-10T-SiO<sup>-</sup> models. The red and blue colors indicate

negative and positive regions, respectively, varying between -42.3 kcal mol<sup>-1</sup> and +23.7 kcal mol<sup>-1</sup>. The molecular graphs of  $\rho(r)$  are also observed

**Table 1** Interaction energies ( $\Delta E_{\text{int}}$ ) of ion-pair (kcal mol<sup>-1</sup>) and main geometrical parameters for different [CTA<sup>+</sup>]-MCM-41 models

	[C <sub>4</sub> TA <sup>+</sup> ]-6T_SiO <sup>-</sup>	[C <sub>6</sub> TA <sup>+</sup> ]-10T_SiO <sup>-</sup>
$\Delta E_{\text{int}}$ B3LYP	-257.7	-232.3
$\Delta E_{\text{int}}$ B3LYP-D3	-268.4	-243.3
Distances (Å)		
O <sub>1</sub> ...N <sub>1</sub>	3.06	3.07
O <sub>2</sub> ...N <sub>2</sub>	3.08	3.06
N <sub>1</sub> ...N <sub>2</sub>	6.36	7.19
C <sub>1</sub> ...C <sub>1</sub>	4.96	4.17
H <sub>1</sub> ...H <sub>1</sub>	6.00	5.00
Angles (°)		
Si <sub>1</sub> -O <sub>1</sub> ...N <sub>1</sub>	166	158
Si <sub>2</sub> -O <sub>2</sub> ...N <sub>2</sub>	152	162
Si <sub>1</sub> ...O <sub>3</sub> ...Si <sub>2</sub>	142	149
N <sub>1</sub> ...O <sub>3</sub> ...N <sub>2</sub>	69	88

the catalytic system, and it have been previously used in heterogeneous catalysis in order to predict interactions between the adsorbate and the catalyst [26, 27]. Also, previous studies of reactions on zeolites showed that the stabilization and formation of intermediates and transition states, depend on the availability of electrons on the surface and the electronic availability plays a crucial role to stabilize the formed species [23, 28, 29].

MEPs show that when the surfactant chain has four or six carbon atoms, no significant differences are observed, so the size of the chain does not influence beyond four carbons (Fig. 3). From experimental viewpoint, it was suggested that as the mesopores are occluded, the reaction occurs at the pore mouth [5]. According to the MEPs, we suggest that the surface of the (CTA<sup>+</sup>)(≡SiO<sup>-</sup>) ion-pair depicts the pore mouth. From the MEPs analysis, it can be also predicted the adsorption sites for reactant molecules and their possible orientation. It is observed, a high electronic availability localized over the oxygen atoms of the ≡SiO<sup>-</sup> groups (red regions) where the electron density is concentrated, while the areas with the most positive electrostatic potential (blue region) is localized over the hydrogens of the -CH<sub>2</sub> groups adjacent (C<sub>β</sub>) to the nitrogens of C<sub>n</sub>TA<sup>+</sup> cation. Thus, this qualitative analysis gives an idea of the adsorption sites of the ion-pair surface and where the methanol and ethyl acetate (EtAc) will be adsorbed more suitable. It is expected that the carbonyl oxygen of EtAc molecule is oriented towards the sites of higher positive potential, while the hydroxyl of methanol is directed towards the regions of the higher negative potential on the surface of the catalyst or at the pore mouth.

Table 2 reports the experimental and calculated vibrational frequencies of [CTA<sup>+</sup>]-MCM-41 before and after calcination, and Fig. 4 shows their correspondents FTIR

spectra. In this figure are also indicated calculated peak positions (in red). After calcination, the bands ascribed to the structure-directing agent CTA<sup>+</sup>, located in the region between 2923 cm<sup>-1</sup> ( $\nu_{\text{as}}\text{CH}_3$ ), 2850 ( $\nu_{\text{s}}\text{CH}_3$ ) and 1478 cm<sup>-1</sup> ( $\delta\text{CH}_3$ ) disappear, indicating that the calcination process was effective in removing the surfactant. Also, multiple bands are visible in the region of 1058 to 792 cm<sup>-1</sup> due to fundamental lattice vibrations (Si-O-Si) [30]. The vibrational bands at 1058 and 1036 cm<sup>-1</sup> are assigned to  $\nu_{\text{as}}\text{Si-O-Si}$  (calcined and non-calcined forms) [31]. The calculated frequencies with both models differ from the experimental frequencies values by about 48 cm<sup>-1</sup> for calcined and up to 169 cm<sup>-1</sup> for non-calcined catalyst. For the hydroxylated silica model  $\nu\text{OH}$  is found at 3736 and 3739 cm<sup>-1</sup> for 6T and 10T models respectively in accordance with previous values reported using a periodic model. [32] Experimental value is not reported because the amount of silanol groups observed should be low, since the removal of the surfactant by calcination produces a smaller number of silanol groups than when it is eliminated by leaching in the presence of solvents. According to several experimental work, numerous synthesized pure silica MCM-41 have this band centered in the region of 3747 to 3744 cm<sup>-1</sup> [33].

Comparison of the relative intensities ( $I_{\text{IR}}$ ) of experimental and theoretical bands (Table 2) showed that in general, both values are very close, except for the  $\nu_{\text{s}}\text{CH}_3$  vibrational mode with a maximum variation of 54.1 for 6T model. The discrepant values probably are related to intermolecular interactions. In general, calculated frequencies and relative IR intensities support the interpretation of the experimental FTIR spectra, because of both values show very close comparative results. In addition, the calculated bands are always present in the experimental spectra, in particular for the calcined catalyst, which serves to validate the cluster models used in this work.

### 3.3 Reaction Mechanism for Basic Heterogeneous Catalyst

It has been postulated that the mechanism for heterogeneous catalysis should be similar to that of homogeneous catalysis [34]. The notions of nucleophilic and electrophilic properties of the reactants (carbonyl group of triglyceride and hydroxyl of alcohol) are related to the transesterification reaction mechanisms. In homogeneous basic catalysis, the key factor of the reaction involves the formation of the nucleophilic alkoxide from the alcohol that will attack the electrophilic carbonyl group of the triglyceride and generates an unstable tetrahedral intermediate that will give rise to the alkyl ester and the corresponding diglyceride anion [35, 36]. The last step involves the recovery of the catalyst proton. This mechanism is repeated for the

**Table 2** Vibrational frequencies ( $\omega$ ,  $\text{cm}^{-1}$ ) and relative IR intensities ( $I_{\text{IR}}$ , %) for calcined and non-calcined. Experimental and theoretical values calculated at B3LYP/6-31G(D,P) level for 6T and 10T models

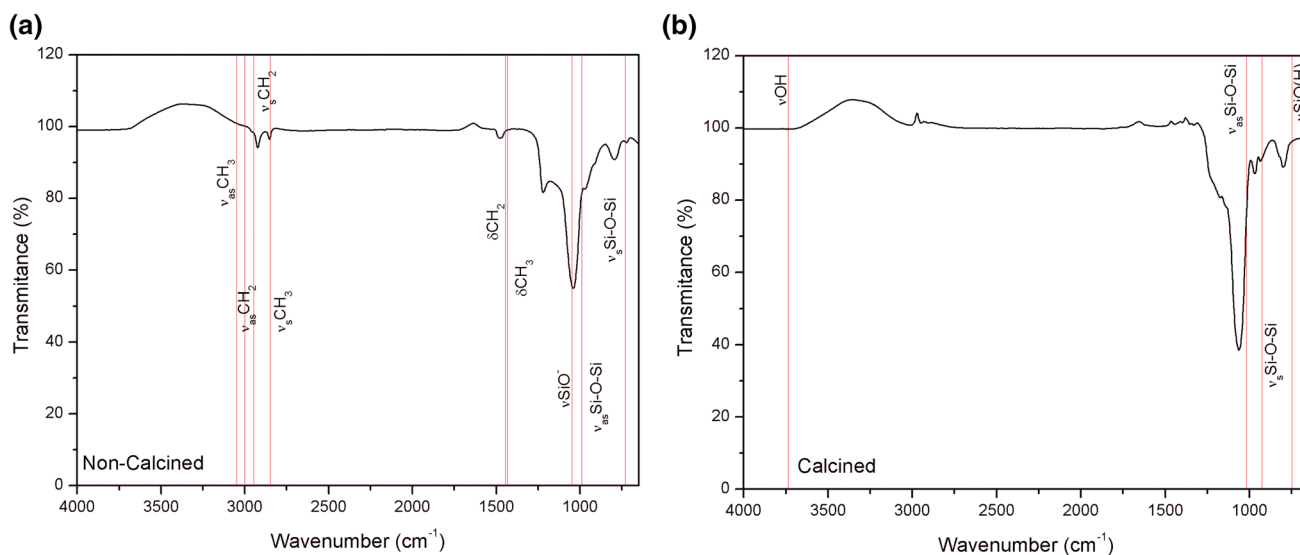
Vibrational mode <sup>c</sup>	Non-calcined [CTA <sup>+</sup> ]Si-MCM-41 <sup>a</sup>									Calcined Si-MCM-41 <sup>b</sup>								
	Experimental		6T			10T			Experimental		6T			10T				
	$\omega$	$I_{\text{IR}}$	$\omega$	$\Delta_{E-T}$	$I_{\text{IR}}$	$\omega$	$\Delta_{E-T}$	$I_{\text{IR}}$	$\omega$	$I_{\text{IR}}$	$\omega$	$\Delta_{E-T}$	$I_{\text{IR}}$	$\omega$	$\Delta_{E-T}$	$I_{\text{IR}}$		
$\nu_{\text{OH}}$	–	–	–	–	–	–	–	–	–	–	3736	–	91.7	3739	–	94.5		
$\nu_{\text{SiO}^-}$	1212	82.8	1049	163	64.5	1043	169	0.0	–	–	–	–	–	–	–	–		
$\nu_{\text{SiO(H)}}$	–	–	–	–	–	–	–	–	969	88.1	927	42	91.0	921	48	91.9		
$\nu_{\text{as}}\text{Si-O-Si}$	1036	56.2	990	46	71.9	1082	–46	42.0	1058	39.1	1084	–26	42.8	1086	–28	44.3		
$\nu_{\text{s}}\text{Si-O-Si}$	792	91.6	730	62	94.0	671	121	95.6	792	90.0	747	45	99.7	754	38	90.1		
$\delta\text{Si-O-Si}$	–	–	442	–	93.0	442	–	87.4	–	–	424	–	90.3	430	–	91.1		
$\nu_{\text{as}}\text{CH}_3$	2923	94.9	3004	–81	90.1	3006	–83	91.0	–	–	–	–	–	–	–	–		
$\nu_{\text{s}}\text{CH}_3$	2850	97.2	2847	3	43.1	2804	46	75.0	–	–	–	–	–	–	–	–		
$\nu_{\text{as}}\text{CH}_2$	2923	94.9	2988	–65	96.3	2950	–27	98.8	–	–	–	–	–	–	–	–		
$\nu_{\text{s}}\text{CH}_2$	2850	97.2	2947	–97	95.4	2910	–60	93.4	–	–	–	–	–	–	–	–		
$\delta\text{CH}_3$	1478	97.5	1433	45	99.7	1383	95	98.0	–	–	–	–	–	–	–	–		
$\delta\text{CH}_2$	1478	97.5	1446	32	99.9	1468	10	99.6	–	–	–	–	–	–	–	–		
Not identified	955	82.8	–	–	–	–	–	–	–	–	–	–	–	–	–	–		
	711	95.9	–	–	–	–	–	–	–	–	–	–	–	–	–	–		

$\Delta_{E-T}$  calculated as the difference between experimental and theoretical values

<sup>a</sup>For non-calcined [CTA<sup>+</sup>]Si-MCM-41, 6T and 10 T refer to [C<sub>4</sub>TA<sup>+</sup>]-6T\_SiO<sup>–</sup> and [C<sub>6</sub>TA<sup>+</sup>]-10T\_SiO<sup>–</sup> models

<sup>b</sup>For calcined Si-MCM-41, 6T refers to 6T\_SiOH and 10T to 10T\_SiOH models

<sup>c</sup> $\nu$ : stretching,  $\nu_{\text{as}}$ : asymmetrical stretching,  $\nu_{\text{s}}$ : symmetrical stretching,  $\delta$ : bending


**Fig. 4** Experimental FTIR spectra (in black) and calculated peak positions for 6T model (in red) for **a** [CTA<sup>+</sup>]-MCM-41 before and **b** after calcination, respectively

division of each fatty acid ester and finally three esters of fatty acids and one molecule of glycerol are formed [37].

For heterogeneous basic catalysis, adsorption of reagents and desorption of products must take place on the catalyst

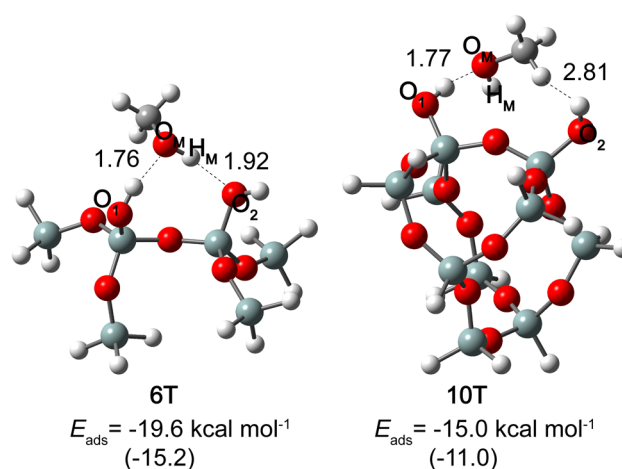
surface in order to the reaction will proceed further. Two hypotheses are postulated for the theoretical study of the reaction mechanism:

- (i.) Single site mechanism: methanol adsorption on the surface of catalyst, activation and formation of methoxide ion by proton transfer, then the methoxide ion attacks the positively polarized carbon of triglyceride (Eley–Rideal type, ER).
- (ii.) Dual site mechanism: both reactants are adsorbed on two sites of the catalyst surface in a concerted way. The reaction occurs with the two adsorbed species and generates an unstable tetrahedral intermediate from the methoxide group and the polarized carbonyl group. (Langmuir–Hinshelwood model, LH).

The first elementary steps shown in Scheme 1 for transesterification reactions of triglycerides are examined next using DFT methods and EtAc and methanol as the illustrative reactants.

### 3.3.1 Single Site Mechanism

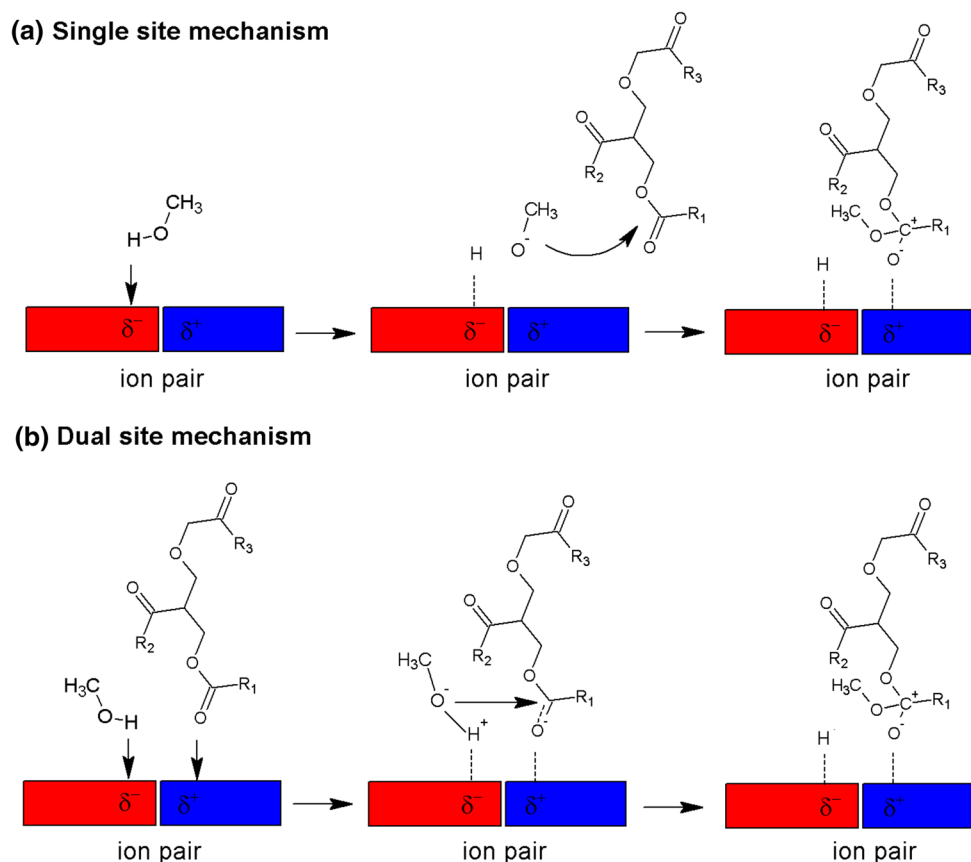
Figures 5 and 6a report the optimized structures for methanol adsorption on calcined catalyst (Si–OH) and non-calcined catalyst [(CTA<sup>+</sup>)(≡SiO<sup>−</sup>) ion-pair], respectively. Table 3 summarizes energies and main geometrical parameters for species involved on the single site mechanism on the surface of non-calcined catalyst.

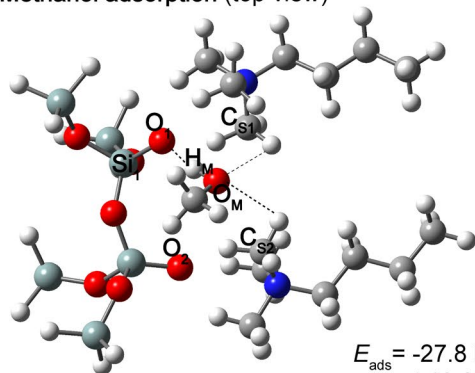


**Fig. 5** Optimized structures for methanol adsorption on hydroxylated MCM-41 (Si–OH). Energy values are also informed

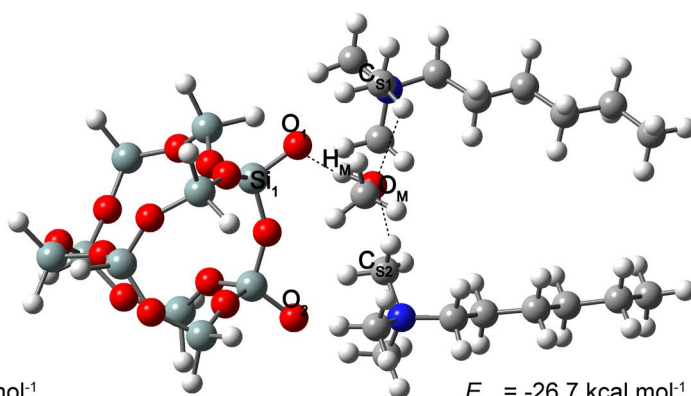
**3.3.1.1 Methanol Adsorption** Results show that the adsorption of methanol on the surface of non-calcined catalyst (ion-pair) is more favorable than adsorption on the calcined catalyst by about 4–6 kcal mol<sup>−1</sup> (6T vs. 10T). The analysis using ion-pair model reveals that methanol can be adsorbed on any of the two available siloxy anions, however

**Scheme 1** Proposed mechanism for the formation of the unstable tetrahedral intermediate involved in transesterification reactions with [CTA<sup>+</sup>]-Si-MCM-41 catalyst

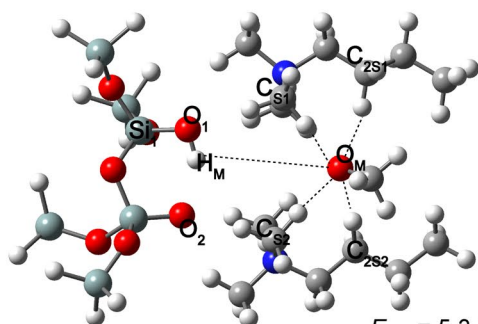


**(a) Methanol adsorption (top view)**


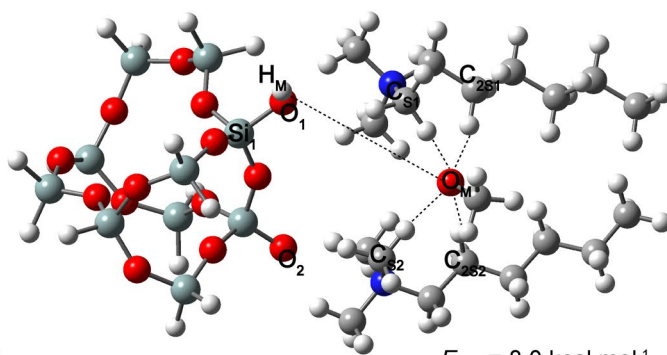
$$E_{\text{ads}} = -27.8 \text{ kcal mol}^{-1} \quad (-19.8)$$



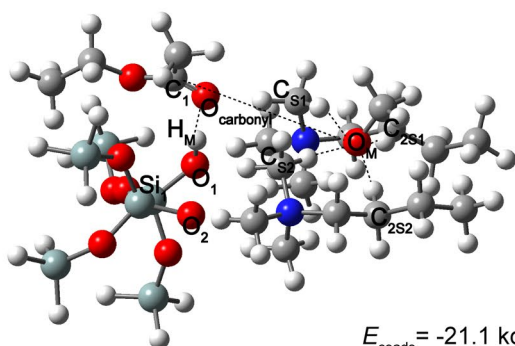
$$E_{\text{ads}} = -26.7 \text{ kcal mol}^{-1} \quad (-17.4)$$

**(b) Adsorbed methoxide (top view)**


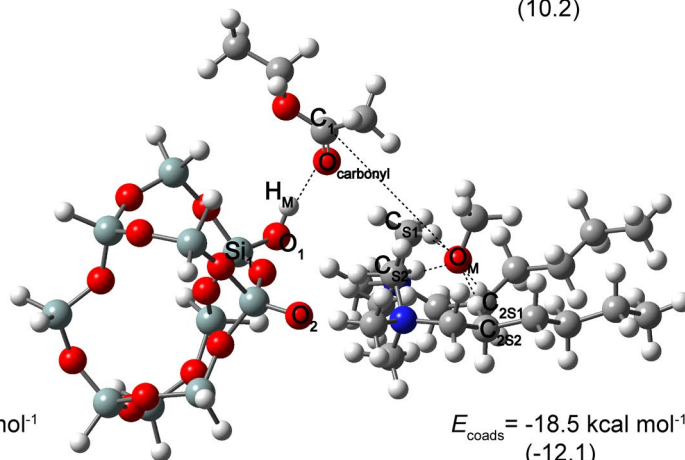
$$E_{\text{DPM}} = 5.3 \text{ kcal mol}^{-1} \quad (7.8)$$



$$E_{\text{DPM}} = 8.0 \text{ kcal mol}^{-1} \quad (10.2)$$

**(c) Ethyl acetate coadsorption (lateral view)**


$$E_{\text{coads}} = -21.1 \text{ kcal mol}^{-1} \quad (-10.7)$$



$$E_{\text{coads}} = -18.5 \text{ kcal mol}^{-1} \quad (-12.1)$$

**Fig. 6** Optimized structures for single site mechanism on the surface of non-calcined catalyst  $[\text{C}_4\text{TA}^+]\text{-6T-SiO}^-$  (left) and  $[\text{C}_6\text{TA}^+]\text{-10T-SiO}^-$  (right), respectively. **a** Methanol adsorption, **b** deprotonation of

methanol and formation of methoxide ion, **c** ethyl acetate coadsorption. Energy values are also informed

methanol adsorption is more favorable on the  $\text{O}_1$  position by about  $6 \text{ kcal mol}^{-1}$  than adsorption on  $\text{O}_2$  atom (results not shown). Also, it is more favorable the methanol adsorption in which the reactant orientates the  $\text{O}_M$  oxygen towards the surfactant chain in the middle of the two  $[\text{CTA}^+]$  cations and the  $\text{H}_M$  hydrogen towards the  $\text{O}_1$  of the siloxy anion. That is, the methanol is adsorbed on the pore mouth. The adsorption energies are similar on both ion-pair models, adsorption on  $[\text{C}_4\text{TA}^+]\text{-6T-SiO}^-$  model is more stable by  $2.4 \text{ kcal mol}^{-1}$

than on  $[\text{C}_6\text{TA}^+]\text{-10T-SiO}^-$  model. The two adsorbed complexes show small differences in interaction distances with the catalyst (Table 3).

As predicted, our results demonstrate that the presence of the ion pair favors the orientation of the  $\text{H}_M$  of methanol towards the negatively charged siloxy anion, while  $\text{O}_M$  is oriented towards the head of the surfactant. This orientation allows the proton transfer of the methanol to the siloxy anion and its subsequent activation to form the methoxide ion as

**Table 3** Energies (kcal mol<sup>-1</sup>), bond distances (Å) and angles (°) between the main atoms of the species involved in the reaction for the single site mechanism on the surface of non-calcined catalyst

	[C <sub>4</sub> TA <sup>+</sup> ]-6T_SiO <sup>-</sup>			[C <sub>6</sub> TA <sup>+</sup> ]-10T_SiO <sup>-</sup>		
	Methanol adsorption	Adsorbed methoxide	EtAc coadsorption	Methanol adsorption	Adsorbed methoxide	EtAc coadsorption
$\Delta E_{\text{B3LYP-D3}}$	-27.8	5.3	-21.1	-26.7	8.0	-18.5
$\Delta E_{\text{B3LYP}}$	-19.8	7.8	-10.7	-17.4	10.2	-12.1
$\Delta H_{\text{B3LYP}}^{\circ}$	-17.8	7.2	-9.8	-15.7	9.1	-10.4
$\Delta G_{\text{B3LYP}}^{\circ}$	-7.3	9.1	-0.1	-5.2	11.1	-0.3
Distances						
O <sub>1</sub> ...O <sub>M</sub>	2.66	4.95	5.20	2.66	5.81	5.88
O <sub>M</sub> ...H <sub>M</sub>	1.00	4.54	4.89	1.01	6.30	5.67
O <sub>1</sub> ...H <sub>M</sub>	1.67	1.00	0.99	1.65	0.96	0.98
O <sub>2</sub> ...H <sub>M</sub>	3.72	1.90	3.54	4.75	5.90	5.48
O <sub>M</sub> ...H(C <sub>S1</sub> ) <sup>a</sup>	2.87	1.96	1.99	2.42	1.93	2.06
O <sub>M</sub> ...H(C <sub>S2</sub> )	2.65	1.95	1.99	2.29	1.98	2.01
O <sub>M</sub> ...H(C <sub>2S1</sub> )	-	2.08	2.06	-	2.00	2.02
O <sub>M</sub> ...H(C <sub>2S2</sub> )	-	2.12	2.14	-	2.09	2.10
O <sub>2</sub> ...H(C <sub>M</sub> )	3.73	-	-	4.82	-	-
O <sub>1</sub> ...N <sub>1</sub>	3.20	3.53	3.50	3.36	3.85	3.85
O <sub>2</sub> ...N <sub>2</sub>	3.09	3.30	3.15	3.12	3.22	3.19
N <sub>1</sub> ...N <sub>2</sub>	6.41	5.98	6.18	6.61	6.05	6.08
C <sub>t</sub> ...C <sub>t</sub>	5.24	5.25	5.26	5.27	4.29	4.21
H <sub>M</sub> ...O <sub>carbonyl</sub>	-	-	1.74	-	-	1.83
O <sub>M</sub> ...C <sub>1</sub>	-	-	5.72	-	-	3.76
Angles						
Si-O <sub>1</sub> ...H <sub>M</sub>	121	101	114	110	112	114
O <sub>M</sub> -H <sub>M</sub> ...O <sub>1</sub>	169	108	102	172	56	97
O <sub>M</sub> -H <sub>M</sub> ...O <sub>2</sub>	97	102	80	94	53	59
O <sub>1</sub> ...O <sub>M</sub> ...O <sub>2</sub>	74	32	41	78	60	54

See Fig. 6 for the identification of atoms

<sup>a</sup>The distance reported is that of the nearest hydrogen atoms of the surfactant

the specie that initiates the transesterification reaction by attacking the electrophilic carbonyl group of ethyl acetate (model of triglyceride).

**3.3.1.2 Deprotonation of Methanol—Formation of Methoxide Ion (Adsorbed Methoxide)** The hydroxylated calcined catalyst (Fig. 5) does not have free electrons to activate methanol, thus deprotonation of methanol to give the alkoxy ion is not favorable for this model. No methoxide ion is found on the hydroxylated calcined catalyst. For the non-calcined catalyst, the Si-O<sup>-</sup> siloxy anion activates the methanol by extraction of the proton and forms Si-OH interacting with the CTA<sup>+</sup> cation. The formed methoxide ion is stabilized by locating in the positive potential zone of the (CTA<sup>+</sup>)(≡SiO<sup>-</sup>) ion pair, that is over both surfactant chains (Fig. 6b). Deprotonation energies are 7.8 and 10.2 kcal mol<sup>-1</sup> for [C<sub>4</sub>TA<sup>+</sup>]-6T\_SiO<sup>-</sup> and [C<sub>6</sub>TA<sup>+</sup>]-10T\_SiO<sup>-</sup> models, respectively. Corrected energies decrease by about 2 kcal mol<sup>-1</sup>. The [C<sub>4</sub>TA<sup>+</sup>]-6T\_SiO<sup>-</sup> model shows lower energy because the smaller O<sub>1</sub>...O<sub>2</sub> distance, that in turns give rise to a H<sub>M</sub>...O<sub>2</sub> hydrogen bond.

Following this mechanism, the next step along the reaction coordinate should involve that the ethyl acetate (without adsorbing) reacts with methoxide ion, or ethyl acetate adsorption and reaction with methoxide ion formed in the first elementary step. If ethyl acetate is coadsorbed, the most stable position involves that the O<sub>carbonyl</sub> is oriented to the Si-OH forming and H-bond (distances H<sub>M</sub>...O<sub>carbonyl</sub> 1.74 Å and 1.83 Å) as can be it can be observed in Fig. 6c, and thus no reaction occurs. If EtAc reacts without adsorbing, the positive potential zone of ion pair is occupied by the methoxy anion (which, in turn, is strongly interacting with the surfactant). Thus, it is postulated that carbonyl activation would not be favorable following this mechanism.

### 3.3.2 Dual Site Mechanism

The existence of a bifunctional site allows the combined adsorption of both reactants. Figure 7 show the structure and Table 4 reports energies and main geometrical parameters

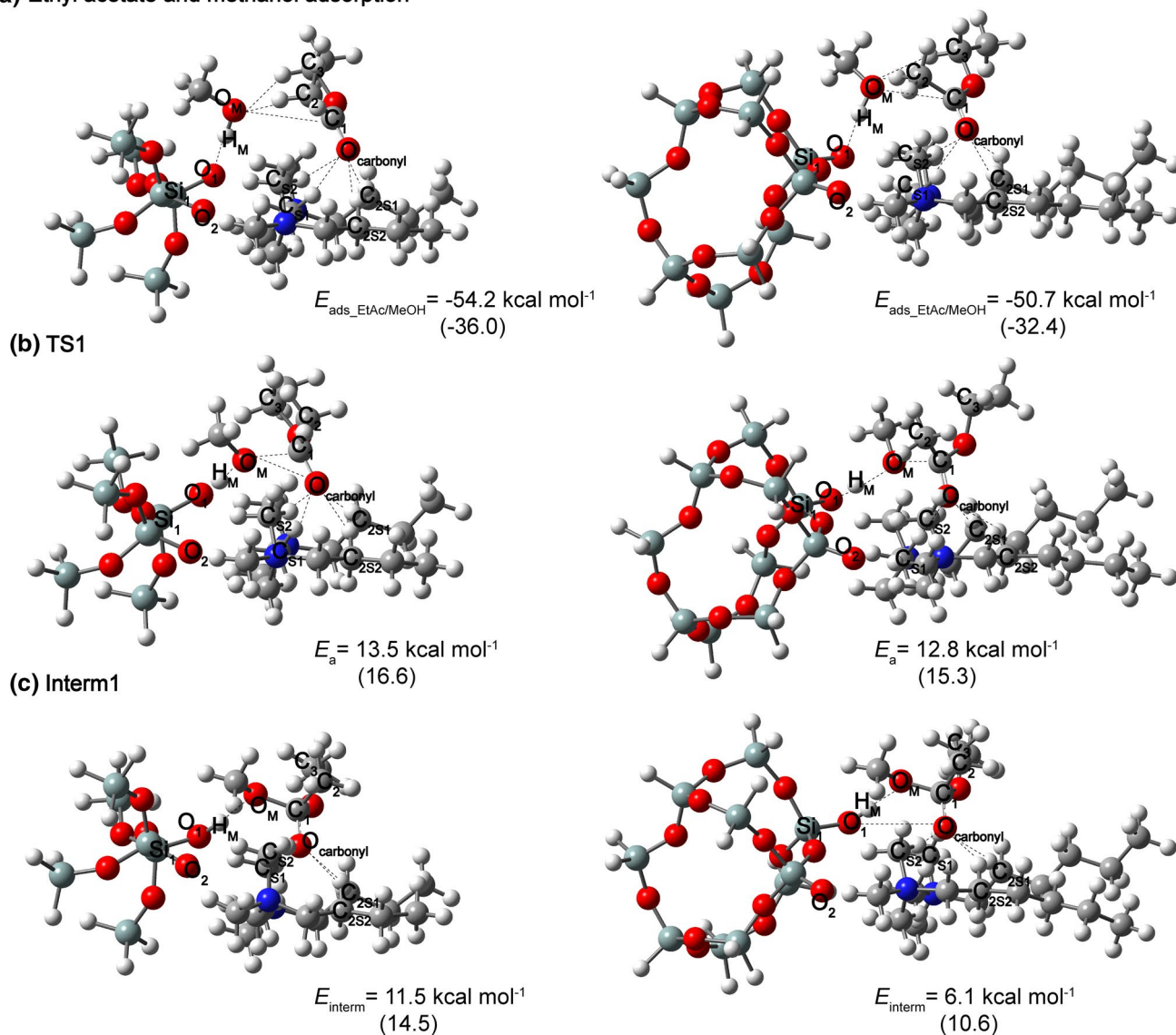
for species involved on the dual site mechanism on the surface of non-calcined catalyst.

**3.3.2.1 Methanol and Ethyl Acetate Adsorption in Concerted Mechanism** According to the bifunctional acid–base mechanism proposed above and described in Scheme 1, it was initially assumed that the carbonyl oxygen of EtAc would interact with the acid site, and methanol would adsorb on the basic site. The optimized geometries of the complexes formed by concerted adsorption of methanol and EtAc on non-calcined Si–MCM-41 are shown in Fig. 7a.

Methanol is adsorbed in the negative potential site of the ion pair (see Fig. 7a), while EtAc is adsorbed by the

carbonyl oxygen in the positive potential site (almost perpendicular and between the two surfactant chains), and thus  $O_M$  is oriented towards  $C_1$  ( $dO_M \cdots C_1 = 3.48 \text{ \AA}$  and  $3.66 \text{ \AA}$ ). These guarantee the proper orientation of methanol and EtAc, in order to allow the interaction that will give rise to the new  $O_M-C_1$  bond. Corrected adsorption energies ( $\Delta E_{\text{ads\_EtAc/MeOH}}$ ) are  $-54.2$  and  $-50.7 \text{ kcal mol}^{-1}$  for  $[C_4TA^+]-6T\_SiO^-$  and  $[C_6TA^+]-10T\_SiO^-$  models respectively. It can be thought that methanol adsorption on basic site ( $-27.8 \text{ kcal mol}^{-1}$  according to single site mechanism) is similar than EtAc adsorption on acid site ( $-26.4 \text{ kcal mol}^{-1}$ , calculated as the difference between

**(a) Ethyl acetate and methanol adsorption**



**Fig. 7** Optimized structures for dual site mechanism on the surface of non-calcined catalyst. **a** Ethyl acetate and methanol adsorption in concerted way, **b** transition state, **c** unstable tetrahedral intermediate. Energy values are also informed

**Table 4** Energies (kcal mol<sup>-1</sup>) and bond distances (Å) between the main atoms of the species involved in the reaction for the dual site mechanism on the surface of non-calcined catalyst

	[C <sub>4</sub> TA <sup>+</sup> ]-6T <sub>-</sub> SiO <sup>-</sup>			[2_C <sub>6</sub> TA <sup>+</sup> ]-10T <sub>-</sub> SiO <sup>-</sup>		
	EtAc/MeOH	TS1	Interm1	EtAc/MeOH	TS1	Interm1
$\Delta E_{\text{B3LYP-D3}}$	-54.2	13.5	11.5	-50.7	12.8	6.1
$\Delta E_{\text{B3LYP}}$	-36.0	16.6	14.5	-32.4	15.3	10.6
$\Delta H_{\text{B3LYP}}^{\circ}$	-31.1	14.1	13.7	-28.9	13.1	9.8
$\Delta G_{\text{B3LYP}}^{\circ}$	-8.8	16.5	15.9	-7.5	18.3	15.8
Distances						
O <sub>M</sub> -H <sub>M</sub>	1.00	1.42	1.71	1.01	1.59	1.83
O <sub>1</sub> ...H <sub>M</sub>	1.64	1.07	1.00	1.60	1.02	0.99
O <sub>M</sub> ...H(C <sub>2</sub> )	2.17	-	-	2.23	-	-
O <sub>M</sub> ...H(C <sub>3</sub> )	2.24	-	-	2.25	-	-
O <sub>M</sub> ...C <sub>1</sub>	3.48	1.92	1.53	3.66	1.90	1.53
C <sub>1</sub> =O <sub>carbonyl</sub>	1.22	1.25	1.29	1.22	1.25	1.29
O <sub>carbonyl</sub> ...H(C <sub>S1</sub> ) <sup>a</sup>	2.31	1.99	1.92	2.32	1.98	1.88
O <sub>carbonyl</sub> ...H(C <sub>S2</sub> )	2.54	2.21	2.35	2.38	2.15	2.10
O <sub>carbonyl</sub> ...H(C <sub>2S1</sub> )	2.57	2.37	2.69	2.63	2.29	2.29
O <sub>carbonyl</sub> ...H(C <sub>2S2</sub> )	2.74	2.93	2.87	2.86	2.78	2.79
O <sub>1</sub> ...C <sub>1</sub>	4.93	3.91	3.78	4.86	4.20	3.91
O <sub>1</sub> ...N <sub>1</sub>	3.26	3.70	3.76	3.31	3.82	3.91
O <sub>2</sub> N <sub>2</sub>	3.09	3.10	3.13	3.09	3.14	3.17
N <sub>1</sub> ...N <sub>2</sub>	6.17	6.34	6.40	6.65	6.57	6.28
C <sub>1</sub> ...C <sub>t</sub>	5.48	5.48	5.22	4.65	4.72	4.63

See Fig. 7 for the identification of atoms

<sup>a</sup>The distance reported is that of the nearest hydrogen atoms of the surfactant

$\Delta E_{\text{ads\_EtAc/MeOH}}$  and  $\Delta E_{\text{ads\_MeOH}}$ ), thus both acid and basic site have similar strength.

The adsorbed complexes are stabilized by hydrogen bonding interactions, where the H<sub>M</sub> interacts with O<sub>1</sub> of silica anion separated by a distance shorter than the sum of the van der Waals radii (distances O<sub>1</sub>...H<sub>M</sub> 1.64 and 1.60 Å for [C<sub>4</sub>TA<sup>+</sup>]-6T<sub>-</sub>SiO<sup>-</sup> and [C<sub>6</sub>TA<sup>+</sup>]-10T<sub>-</sub>SiO<sup>-</sup> models), at the same time O<sub>M</sub> interacts with hydrogen atoms of EtAc [H(C<sub>2</sub>) and H(C<sub>3</sub>)]. Also, carbonyl oxygen atom of EtAc interacts with both head and tail of both surfactant molecules with distances between 2.3 and 2.5 Å [O<sub>carbonyl</sub>...H(C<sub>S1</sub>) and O<sub>carbonyl</sub>...H(C<sub>S2</sub>)] and 2.6–2.9 Å [O<sub>carbonyl</sub>...H(C<sub>2S1</sub>) and O<sub>carbonyl</sub>...H(C<sub>2S2</sub>)]. See Fig. 7a and Table 4).

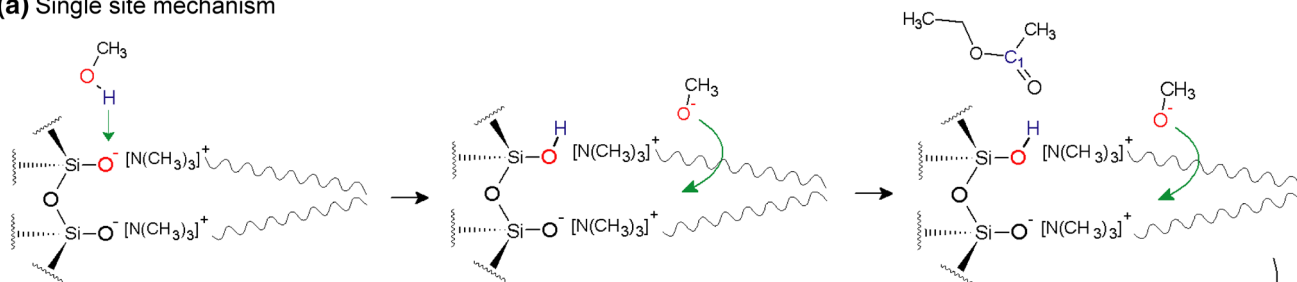
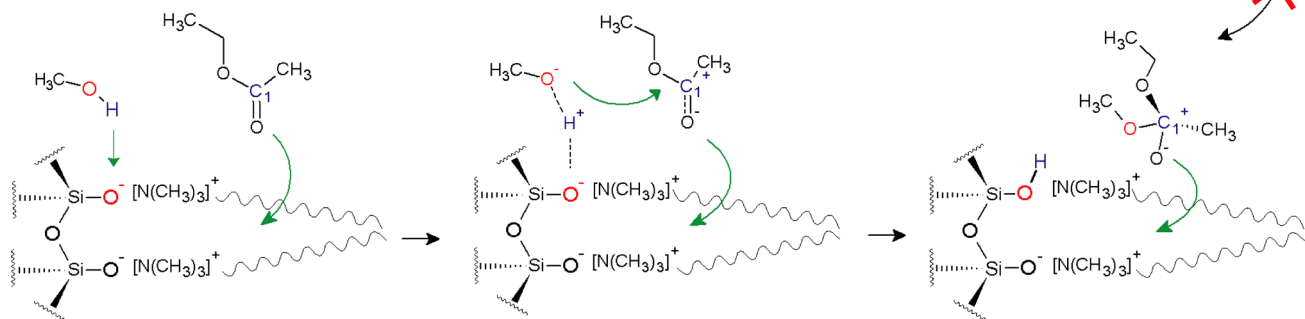
**3.3.2.2 Transition State** In the transition state (Fig. 7b), the bond breakage and transfer of the proton of methanol to the ≡SiO<sup>-</sup> anion and attack of methoxide anion to the carbonyl carbon of the EtAc occur simultaneously in concerted way. The C=O bond is strongly polarized on the acid center of both surfactant molecules (distances C<sub>1</sub>=O<sub>carbonyl</sub>=1.25 Å), and the C<sub>1</sub> acquire a net positive charge becoming electrophilic. This polarization makes this carbon atom more susceptible to be attacked by the methoxide anion formed on the Lewis site. Thus, both acid and basic sites play a cooperative key role, the basic center polarizes the adsorbed methanol and the acid center

polarizes the carbonyl of adsorbed EtAc to yield a transition state that involves a concerted reaction to yield the intermediate. The imaginary frequency is related to the proton transfer of MeOH to the siloxy anion and the attack of O<sub>M</sub> to the C<sub>1</sub> carbon of EtAc. The corrected calculated activation energies are 13.5 and 12.8 kcal mol<sup>-1</sup> for the two non-calcined catalyst models.

At the TS the O<sub>M</sub>-H<sub>M</sub> distance increases to 1.4–1.6 Å and O<sub>1</sub>...H<sub>M</sub> decreases to 1.1–1.0 Å, reflecting the beginning of the proton transfer from methanol to siloxy anion. At the same time, O<sub>M</sub>...C<sub>1</sub> distance decreases from 3.5–3.6 Å in the adsorbed complex to 1.9 Å in the TS1 for both models catalyst. Distances are slightly shorter in the case of 10T model.

**3.3.2.3 Reaction intermediate** The obtained intermediate (Interm1) is positioned mainly above the head of both surfactant molecules. This reaction intermediate is only 2 and 6.7 kcal mol<sup>-1</sup> more stable than the transition state {[C<sub>4</sub>TA<sup>+</sup>]-6T<sub>-</sub>SiO<sup>-</sup> and [C<sub>6</sub>TA<sup>+</sup>]-10T<sub>-</sub>SiO<sup>-</sup> models}. In this intermediate, the O<sub>M</sub>...C<sub>1</sub> bond is 1.53 Å and the C=O bond is elongated to 1.29 Å. The low stability of the reaction intermediate can be explained by the repulsive interactions between the two methyl groups of both surfactant heads [-N(CH<sub>3</sub>)<sub>3</sub>]<sup>+</sup>.

An additional step implies that the Interm1 moves towards to both surfactant tails to give to another

**(a) Single site mechanism****(b) Dual site mechanism**

**Scheme 2** Formation of the tetrahedral intermediate by: **a** Single site mechanism, **b** Dual site mechanism

intermediate which differs only 2 kcal mol<sup>-1</sup> in energies. In general, the Interm2 is quite similar to Interm1, for 6T model the main difference between the two intermediate complexes is found in the O<sub>M</sub>⋯C<sub>1</sub> distance (dO<sub>M</sub>⋯C<sub>1</sub> = 1.50 Å) and in C<sub>M</sub>-O<sub>M</sub>⋯C<sub>1</sub>-C<sub>1</sub>-C<sub>methyl</sub> dihedral angle (-47° and -78°, respectively).

Thus, a tetrahedral intermediate from the attack of the electrophilic carbon atom by nucleophilic methoxide is produced. The breakdown of this unstable intermediate will give rise to the products.

Summing up, following this dual site reaction mechanism, the relative orientation of both molecules is very favorable for the transesterification reaction occurs. It is interesting to note, that as the reaction progresses, the methyl groups of the trimethylamine are rearranged and rotated for a better fit of the adsorbed species. Also, along the reaction coordinate, it can be observed that the O<sub>carbonyl</sub> atom of the C=O bond in Ethyl Acetate is interacting with four hydrogens atoms of both surfactant molecules, with calculated O<sub>carbonyl</sub>⋯H distances between 1.9 and 2.9 Å (Table 4).

A detailed scheme tying together a summary of the two proposed mechanisms are shown in Scheme 2.

## 4 Conclusions

In this work, a theoretical study in conjunction with a spectroscopic analysis by FTIR were carried out in order to obtain molecular insights on the role of (CTA<sup>+</sup>)(SiO<sup>-</sup>) ion

pair into the catalytic activity of [CTA<sup>+</sup>]-Si-MCM-41. Our results show that the formation of the ionic pair is fundamental for the catalytic activity. The joint analysis of FTIR spectroscopy and DFT calculations reveal that the interaction between the basic site of the silica surface (≡SiO<sup>-</sup>) and the surfactant molecule (CTA<sup>+</sup>) generate a bifunctional catalytic site, with acid and basic characteristics. The catalyst was modeled with a model whose reliability was assessed by comparison with FTIR spectra.

The most favorable mechanism involved in the transesterification reaction of EtAc with methanol on [CTA<sup>+</sup>]-Si-MCM-41 catalyst is the dual site mechanism. Moreover, the dual site reaction mechanism relates to the catalytic activity of the [CTA<sup>+</sup>]-Si-MCM-41 catalyst with the presence of the (CTA<sup>+</sup>)(≡SiO<sup>-</sup>) ion pair. The basic center polarizes the adsorbed methanol and the acid center polarizes the carbonyl of adsorbed EtAc. Thus, this catalytic site makes possible the simultaneous adsorption of both reactants at the pore mouth and generates a concerted transition state that gives rise to the beginning of the transesterification reaction. Moreover, with the loss of CTA<sup>+</sup> by calcination, the reaction no progress and theoretical calculations showed that the hydroxylated calcined catalyst could not activate the methanol, thus no catalytic activity was observed. In other words, we conclude that in the absence of CTA<sup>+</sup> the Si-MCM-41 not show catalytic activity. Besides, theoretical results are in good agreement with experimental values.

Finally, our results suggest that the O<sup>-</sup>⋯[N(CH<sub>3</sub>)<sub>3</sub>]<sup>+</sup> interaction between (≡SiO<sup>-</sup>) and (CTA<sup>+</sup>) is a key interaction in

the strong basicity of oxygen atoms at siloxy groups and this fact show to be a way promising for the design of new basic catalyst. Further studies on the nature of interactions on these systems are under investigation in our laboratory, and results will be published in the near future.

**Acknowledgements** The authors acknowledge to Secretaría General de Ciencia y Técnica de la Universidad Nacional del Nordeste (Grant No. F017-2014 and Grant Nos. 18V002, SGCyT-UNNE), and Consejo Nacional de Investigaciones Científicas y Técnicas (Grant No. PIP-0678 CONICET) of Argentina for financial support. H. J. Alves gratefully acknowledges the Araucária Foundation (State of Paraná Research Foundation) for its financial support (Grant No. 465/2010—Protocol 18028).

## References

- Lee AF, Bennett JA, Manayil JC, Wilson K (2014) Heterogeneous catalysis for sustainable biodiesel production via esterification and transesterification. *Chem Soc Rev* 43(22):7887–7916. <https://doi.org/10.1039/C4CS00189C>
- Grün M, Unger KK, Matsumoto A, Tsutsumi K (1999) Novel pathways for the preparation of mesoporous MCM-41 materials: control of porosity and morphology. *Microporous Mesoporous Mater* 27(2):207–216. [https://doi.org/10.1016/S1387-1811\(98\)00255-8](https://doi.org/10.1016/S1387-1811(98)00255-8)
- Fabiano DP, Hamad B, Cardoso D, Essayem N (2010) On the understanding of the remarkable activity of template-containing mesoporous molecular sieves in the transesterification of rapeseed oil with ethanol. *J Catal* 276(1):190–196. <https://doi.org/10.1016/j.jcat.2010.09.015>
- Kubota Y, Nishizaki Y, Ikeya H, Saeki M, Hida T, Kawazu S, Yoshida M, Fujii H, Sugi Y (2004) Organic–silicate hybrid catalysts based on various defined structures for Knoevenagel condensation. *Microporous Mesoporous Mater* 70(1):135–149. <https://doi.org/10.1016/j.micromeso.2004.02.017>
- Martins L, Bonagamba TJ, de Azevedo ER, Bargiela P, Cardoso D (2006) Surfactant containing Si-MCM-41: an efficient basic catalyst for the Knoevenagel condensation. *Appl Catal A Gen* 312(Supplement C):77–85. <https://doi.org/10.1016/j.apcat.a.2006.06.035>
- Ranucci CR, Colpini LMS, Monteiro MR, Kothe V, Gasparini LJ, Alves HJ (2015) Preparation, characterization and stability of KF/Si-MCM-41 basic catalysts for application in soybean oil transesterification with methanol. *J Environ Chem Eng* 3(2):703–707. <https://doi.org/10.1016/j.jece.2015.02.023>
- Kubota Y, Nishizaki Y, Sugi Y (2000) High catalytic activity of as-synthesized, ordered porous silicate-quaternary ammonium composite for Knoevenagel condensation. *Chem Lett* 29(9):998–999. <https://doi.org/10.1246/cl.2000.998>
- Kubota Y, Sugi Y, Tatsumi T (2007) Organic-inorganic hybrid catalysts based on ordered porous structures for carbon-carbon bond forming reactions. *Catal Surv Asia* 11(4):158–170. <https://doi.org/10.1007/s10563-007-9030-4>
- Martins L, Cardoso D (2007) Influence of surfactant chain length on basic catalytic properties of Si-MCM-41. *Microporous Mesoporous Mater* 106(1):8–16. <https://doi.org/10.1016/j.micromeso.2007.01.037>
- Kothe V, Alves HJ, Silveira MHL, Pereira L (2016) Synthesis, characterization and application of [CTA+]/MCM-41 in the catalytic conversion of soybean oil to fatty acid methyl esters. *J Adv Chem* 12(6):4117–4126. <https://doi.org/10.24297/jac.v12i6.4348>
- Gomes GJ, Zalazar MF, Lindino CA, Scremin FR, Bittencourt PRS, Costa MB, Peruchena NM (2017) Adsorption of acetic acid and methanol on H-Beta zeolite: an experimental and theoretical study. *Microporous Mesoporous Mater* 252:17–28. <https://doi.org/10.1016/j.micromeso.2017.06.008>
- Gomes GJ, Zalazar MF, Arroyo PA, Scremin FR, Costa MB, Bittencourt PRS, Lindino CA, Peruchena NM (2019) Molecular-level understanding of the rate-determining step in esterification reactions catalyzed by H-ZSM-5 zeolite. An experimental and theoretical study. *ChemistrySelect* 4:3031–3041. <https://doi.org/10.1002/slct.201900689>
- Gierada M, Petit I, Handzlik J, Tielens F (2016) Hydration in silica based mesoporous materials: a DFT model. *Phys Chem Chem Phys* 18(48):32962–32972. <https://doi.org/10.1039/C6CP05460A>
- Zalazar MF, Duarte DJR, Peruchena NM (2009) Adsorption of alkenes on acidic zeolites. Theoretical study based on the electron charge density. *J Phys Chem A* 113(49):13797–13807. <https://doi.org/10.1021/jp9053814>
- Paul G, Bisio C, Braschi I, Cossi M, Gatti G, Gianotti E, Marchese L (2018) Combined solid-state NMR, FT-IR and computational studies on layered and porous materials. *Chem Soc Rev* 47(15):5684–5739. <https://doi.org/10.1039/C7CS00358G>
- Ugliengo P, Sodupe M, Musso F, Bush IJ, Orlando R, Dovesi R (2008) Realistic models of hydroxylated amorphous silica surfaces and MCM-41 mesoporous material simulated by large-scale periodic B3LYP calculations. *Adv Mater* 20(23):4579–4583. <https://doi.org/10.1002/adma.200801489>
- Becke AD (1993) Density-functional thermochemistry. III. The role of exact exchange. *J Chem Phys* 98(7):5648–5652. <https://doi.org/10.1063/1.464913>
- Lee C, Yang W, Parr RG (1988) Development of the colle-salvetti correlation-energy formula into a functional of the electron density. *Phys Rev B* 37:785–789. <https://doi.org/10.1103/PhysRevB.37.785>
- Frisch MJ, Trucks GW, Schlegel HB, Scuseria GE, Robb MA, Cheeseman JR, Montgomery JA, Vreven T, Kudin KN, Burant JC, Millam JM, Iyengar SS, Tomasi J, Barone V, Mennucci B, Cossi M, Scalmani G, Rega N, Petersson GA, Nakatsuji H, Hada M, Ehara M, Toyota K, Fukuda R, Hasegawa J, Ishida M, Nakajima T, Honda Y, Kitao O, Nakai H, Klene M, Li X, Knox JE, Hratchian HP, Cross JB, Adamo C, Jaramillo J, Gomperts R, Stratmann RE, Yazyev O, Austin AJ, Cammi R, Pomelli C, Ochterski JW, Ayala PY, Morokuma K, Voth GA, Salvador P, Dannenberg JJ, Zakrzewski G, Dapprich S, Daniels AD, Strain MC, Farkas O, Malick DK, Rabuck AD, Raghavachari K, Foresman JB, Ortiz JV, Cui Q, Baboul AG, Clifford S, Cioslowski J, Stefanov BB, Liu G, Liashenko A, Piskorz P, Komaromi I, Martin RL, Fox DJ, Keith T, Al-Laham MA, Peng CY, Nanayakkara A, Challacombe M, Gill PMW, Johnson B, Chen W, Wong MW, Gonzalez C, Pople JA (2009) *Gaussian 09*. revision A.01 edn. Gaussian, Inc., Wallingford
- Gao Y, Chen H, Tay-Agbozo S, Kispert LD (2017) Photo-induced electron transfer of carotenoids in mesoporous sieves (MCM-41) and surface modified MCM-41: the role of hydrogen bonds on the electron transfer. *J Photochem Photobiol A* 341:1–11. <https://doi.org/10.1016/j.jphotochem.2017.03.013>
- Gonzalez C, Schlegel HB (1989) An improved algorithm for reaction path following. *J Chem Phys* 90(4):2154–2161. <https://doi.org/10.1063/1.456010>
- Gonzalez C, Schlegel HB (1990) Reaction path following in mass-weighted internal coordinates. *J Phys Chem* 94(14):5523–5527. <https://doi.org/10.1021/j100377a021>
- Zalazar MF, Peruchena NM (2011) Topological description of the bond breaking and bond forming processes of the alkene protonation reaction in the zeolite chemistry: an AIM study. *J Mol Model* 17(10):2501–2511. <https://doi.org/10.1007/s00894-010-0933-z>

24. Grimme S, Antony J, Ehrlich S, Krieg S (2010) A consistent and accurate ab initio parametrization of density functional dispersion correction (DFT-D) for the 94 elements H-Pu. *J Chem Phys* 132(15):154104. <https://doi.org/10.1063/1.3382344>
25. Keith TA (2013) AIMAll (Version 13.05.06) edn. TK Gristmill Software, Overland Park
26. Zalazar MF, Cabral ND, Romero Ojeda GD, Alegre CIA, Peruchena NM (2018) Confinement effects in protonation reactions catalyzed by zeolites with large void structures. *J Phys Chem C* 122(48):27350–27359. <https://doi.org/10.1021/acs.jpcc.8b07357>
27. Zalazar MF, Paredes EN, Romero Ojeda GD, Cabral ND, Peruchena N (2018) Study of confinement and catalysis effects of the reaction of methylation of benzene by methanol in H-Beta and H-ZSM-5 zeolites by topological analysis of electron density. *J Phys Chem C* 122(6):3350–3362. <https://doi.org/10.1021/acs.jpcc.7b10297>
28. Zalazar MF, Peruchena NM (2007) Topological analysis of the electronic charge density in the ethene protonation reaction catalyzed by acidic zeolite. *J Phys Chem A* 111(32):7848–7859. <https://doi.org/10.1021/jp071659v>
29. Zalazar MF, Peruchena N (2014) Laplacian of the electron density: a hole-lump interaction as a tool to study stereoelectronic control of chemical reactions. *J Phys Org Chem* 27(4):327–335. <https://doi.org/10.1002/poc.3260>
30. Alba MD, Luan Z, Klinowski J (1996) Titanosilicate mesoporous molecular sieve MCM-41: synthesis and characterization. *J Phys Chem* 100(6):2178–2182. <https://doi.org/10.1021/jp9515895>
31. Raji F, Pakizeh M (2013) Study of Hg(II) species removal from aqueous solution using hybrid ZnCl<sub>2</sub>-MCM-41 adsorbent. *Appl Surf Sci* 282:415–424. <https://doi.org/10.1016/j.apsusc.2013.05.145>
32. Comas-Vives A (2016) Amorphous SiO<sub>2</sub> surface models: energetics of the dehydroxylation process, strain, ab initio atomistic thermodynamics and IR spectroscopic signatures. *Phys Chem Chem Phys* 18:7475–7482. <https://doi.org/10.1039/c6cp00602g>
33. Rimola A, Costa D, Sodupe M, Lambert J-F, Ugliengo P (2013) Silica surface features and their role in the adsorption of biomolecules: computational modeling and experiments. *Chem Rev* 113(6):4216–4313. <https://doi.org/10.1021/cr3003054>
34. Di Serio M, Tesser R, Pengmei L, Santacesaria E (2008) Heterogeneous catalysts for biodiesel production. *Energy Fuels* 22(1):207–217. <https://doi.org/10.1021/ef700250g>
35. Schuchardt U, Sercheli R, Vargas RM (1998) Transesterification of vegetable oils: a review. *J Braz Chem Soc* 9:199–210. <https://doi.org/10.1590/S0103-50531998000300002>
36. Endalew AK, Kiros Y, Zanzi R (2011) Inorganic heterogeneous catalysts for biodiesel production from vegetable oils. *Biomass Bioenergy* 35(9):3787–3809. <https://doi.org/10.1016/j.biombioe.2011.06.011>
37. Dimian AC, Srokol ZW, Mittelmeijer-Hazeleger MC, Rothenberg G (2010) Interrelation of chemistry and process design in biodiesel manufacturing by heterogeneous catalysis. *Top Catal* 53(15):1197–1201. <https://doi.org/10.1007/s11244-010-9562-0>

**Publisher's Note** Springer Nature remains neutral with regard to jurisdictional claims in published maps and institutional affiliations.